Kinome profiling of non-Hodgkin lymphoma identifies Tyro3 as a therapeutic target in primary effusion lymphoma

Jason P. Wong[a], Timothy J. Stuhlmiller[b], Louise C. Giffin[a], Carolina Lin[a], Rachele Bigi[a,c], Jichen Zhao[d,e], Weihe Zhang[d,e], Ariana G. Bravo Cruz[a], Steven I. Park[f], H. Shelton Earp[f], Dirk P. Dittmer[a,c], Stephen V. Frye[d,e], Xiaodong Wang[d,e,1], Gary L. Johnson[b,1], and Blossom Damania[a,1]

[a]Department of Microbiology and Immunology and Lineberger Comprehensive Cancer Center, University of North Carolina at Chapel Hill, Chapel Hill, NC 27599; [b]Department of Pharmacology and Lineberger Comprehensive Cancer Center, University of North Carolina School of Medicine, Chapel Hill, NC 27599; [c]Department of Microbiology and Immunology and Center for AIDS Research, University of North Carolina at Chapel Hill, Chapel Hill, NC 27599; [d]Center for Integrative Chemical Biology and Drug Discovery, UNC Eshelman School of Pharmacy, University of North Carolina at Chapel Hill, Chapel Hill, NC 27599; [e]Division of Chemical Biology and Medicinal Chemistry, UNC Eshelman School of Pharmacy, University of North Carolina at Chapel Hill, Chapel Hill, NC 27599; and [f]Department of Medicine and Lineberger Comprehensive Cancer Center, University of North Carolina School of Medicine, Chapel Hill, NC 27599

Edited by Yuan Chang, University of Pittsburgh, Pittsburgh, PA, and approved July 1, 2019 (received for review March 11, 2019)

Non-Hodgkin lymphomas (NHLs) make up the majority of lymphoma diagnoses and represent a very diverse set of malignancies. We sought to identify kinases uniquely up-regulated in different NHL subtypes. Using multiplexed inhibitor bead-mass spectrometry (MIB/MS), we found Tyro3 was uniquely up-regulated and important for cell survival in primary effusion lymphoma (PEL), which is a viral lymphoma infected with Kaposi's sarcoma-associated herpesvirus (KSHV). Tyro3 was also highly expressed in PEL cell lines as well as in primary PEL exudates. Based on this discovery, we developed an inhibitor against Tyro3 named UNC3810A, which hindered cell growth in PEL, but not in other NHL subtypes where Tyro3 was not highly expressed. UNC3810A also significantly inhibited tumor progression in a PEL xenograft mouse model that was not seen in a non-PEL NHL model. Taken together, our data suggest Tyro3 is a therapeutic target for PEL.

KSHV | Tyro3 | kinase | PEL | lymphoma

Non-Hodgkin lymphoma (NHL) consists of many subtypes covering a wide range of characteristics that include differences in cell of origin, aggressiveness, and viral association. One of these NHL subtypes is primary effusion lymphoma (PEL), which is associated with Kaposi's sarcoma-associated herpesvirus (KSHV). Patients with PEL have a median survival time of 6 mo after diagnosis, as standard chemotherapy is generally ineffective in treating PEL (1, 2). Several clinical studies have taken different approaches to treat PEL, and while some have shown promise, there is still no effective treatment for PEL (3). For example, treatment of PEL with bortezomib, a proteasome inhibitor that inhibits NF-κB activity, has shown variable results in clinical trials (4–6). Therefore, there is a need to identify new targeted therapies to treat PEL.

Signaling pathways are often dysregulated in cancer, and kinases that control the propagation of these signaling cascades frequently have aberrant activity. The use of kinase inhibitors to treat cancers has shown clinical efficacy as a single agent or in the adjuvant setting. For example, imatinib, an inhibitor of the BCR-ABL kinase, is efficacious in treating chronic myelogenous leukemia (7). We were interested in identifying kinases that were uniquely activated in PEL in comparison with other NHL subtypes. A kinase with unique or significantly higher activity in PEL compared with other NHL subtypes may indicate that PEL is dependent on the signaling activity of that particular kinase compared with other NHL subtypes.

We decided to compare PEL to 4 other B cell NHL subtypes: follicular lymphoma (FL), diffuse large B cell lymphoma (DLBCL), mantle cell lymphoma (MCL), and Burkitt's lymphoma (BL). These subtypes are derived from different stages of B cell development that include the mantle zone, germinal center, and postgerminal center (8–13). As different B cell NHL subtypes may arise during different stages of normal B cell development, there are likely to be differences in the expressed kinome (14). Two of the subtypes (BL and PEL) are commonly associated with viral infection. BL is associated with Epstein-Barr virus (EBV) infection, while PEL is distinguished by Kaposi's sarcoma-associated herpesvirus (KSHV) infection (15–17). Coinfection with EBV is also common in PEL (18–20). By examining an array of NHL subtypes that are derived from different stages of B cell development, and being virally associated or not, we intended to capture a wide enough spread in cellular phenotypes to identify distinct kinases which are activated or repressed in PEL in comparison with other B cell NHL subtypes.

Significance

B cell-derived non-Hodgkin lymphomas (NHLs) consist of a very diverse set of malignancies. One NHL subtype, primary effusion lymphoma (PEL), has a poor prognosis with patients having a median survival time of about 6 mo postdiagnosis. By profiling the kinome of multiple B cell NHL lines, we identified several kinases uniquely upregulated in PEL compared with other subtypes, the most significant of which was Tyro3. We developed an inhibitor against Tyro3 kinase activity; this small molecule inhibitor reduced PEL survival and growth in vitro, and tumor burden in a PEL xenograft model in vivo. Our study suggests that a Tyro3 inhibitor may be beneficial in treating PEL.

Author contributions: J.P.W., S.I.P., and B.D. designed research; J.P.W., T.J.S., L.C.G., C.L., and A.G.B.C. performed research; R.B., J.Z., W.Z., H.S.E., S.V.F., and X.W. contributed new reagents/analytic tools; J.P.W., T.J.S., D.P.D., X.W., G.L.J., and B.D. analyzed data; and J.P.W., T.J.S., S.V.F., X.W., G.L.J., and B.D. wrote the paper.

Conflict of interest statement: X.W., W.Z., H.S.E., and S.V.F. have filed a patent on UNC3810A. X.W., H.S.E., and S.V.F. hold stock in Meryx Inc.

This article is a PNAS Direct Submission.

Data deposition: The RNA-seq data reported in this study are deposited in the Gene Expression Omnibus database under the accession number GSE114791. The mass spectrometry proteomics data from the MIB/MS profiling are deposited to the ProteomeXchange Consortium by the PRIDE (79) partner repository with the dataset identifier PXD012087.

[1]To whom correspondence may be addressed. Email: damania@med.unc.edu, gary_johnson@med.unc.edu, or xiaodonw@email.unc.edu.

This article contains supporting information online at www.pnas.org/lookup/suppl/doi:10.1073/pnas.1903991116/-/DCSupplemental.

Results

The Functional Cellular Kinome Is More Similar within a NHL Subtype than across Subtypes. To identify potential vulnerabilities within subtypes of lymphoma, we performed multiplexed inhibitor bead-mass spectrometry (MIB/MS) kinome profiling on 24 individual cell lines in biological triplicate as well as in primary B cells from healthy donors (21). The cellular lysate was run through a column containing beads attached with different kinase inhibitors, which bind and capture functionally expressed kinases. The bound kinases are eluted off and then identified and quantified using mass spectrometry. Replicate MIB/MS runs were consistent and were averaged and compared with freshly harvested primary B cells from 5 donors (*SI Appendix*, Fig. S1 and Dataset S1) (22). From all MIB/MS experiments combined, 385 kinases were identified in at least 1 cell line, and 151 kinases were commonly captured from all cell lines. Kinase names are derived from the Uniprot naming nomenclature (with their official corresponding gene name provided in Dataset S2). Euclidian hierarchical clustering of all MS data demonstrated that kinome profiles of lymphoma cell lines generally clustered them according to subtype, with the PEL subtype being the most distinct (Fig. 1*A*). Though FL is generally indolent, it can progress, and in some cases transform into DLBCL (23, 24). Notably, there were several cell lines (SuDHL4, Karpas422, and WSU-NHL), which have been characterized as either FL or DLBCL (25–30). Since WSU-NHL clustered with the other DLBCLs, and SuDHL4 and Karpas422 with the other FL, we categorized them as such, respectively (Fig. 1*A*). Three kinases were captured in all cancer cell lines but were absent from primary B cells: STK6 (Aurora kinase A), NEK2, and MK06 (ERK3) (Fig. 1*B*). Other kinases with greater MIB binding in NHL compared with primary B cells were associated with cell cycle regulation (CDK1, CHK1, PLK1, PMYT1, and AURKB) (Fig. 1*B*). Comparing subtypes to one another, some kinases displayed a bias toward having greater or less MIB binding in a particular subtype versus others. For example, KS6B1 (p70 S6K) showed the greatest MIB binding in PEL (Fig. 1*C*). Conversely, ATR displayed less MIB binding in MCL and DLBCL versus the other subtypes (Fig. 1*D*). LIMK2 also displayed the greatest MIB binding in DLBCL (Fig. 1*E*), while PKN1 was captured the least

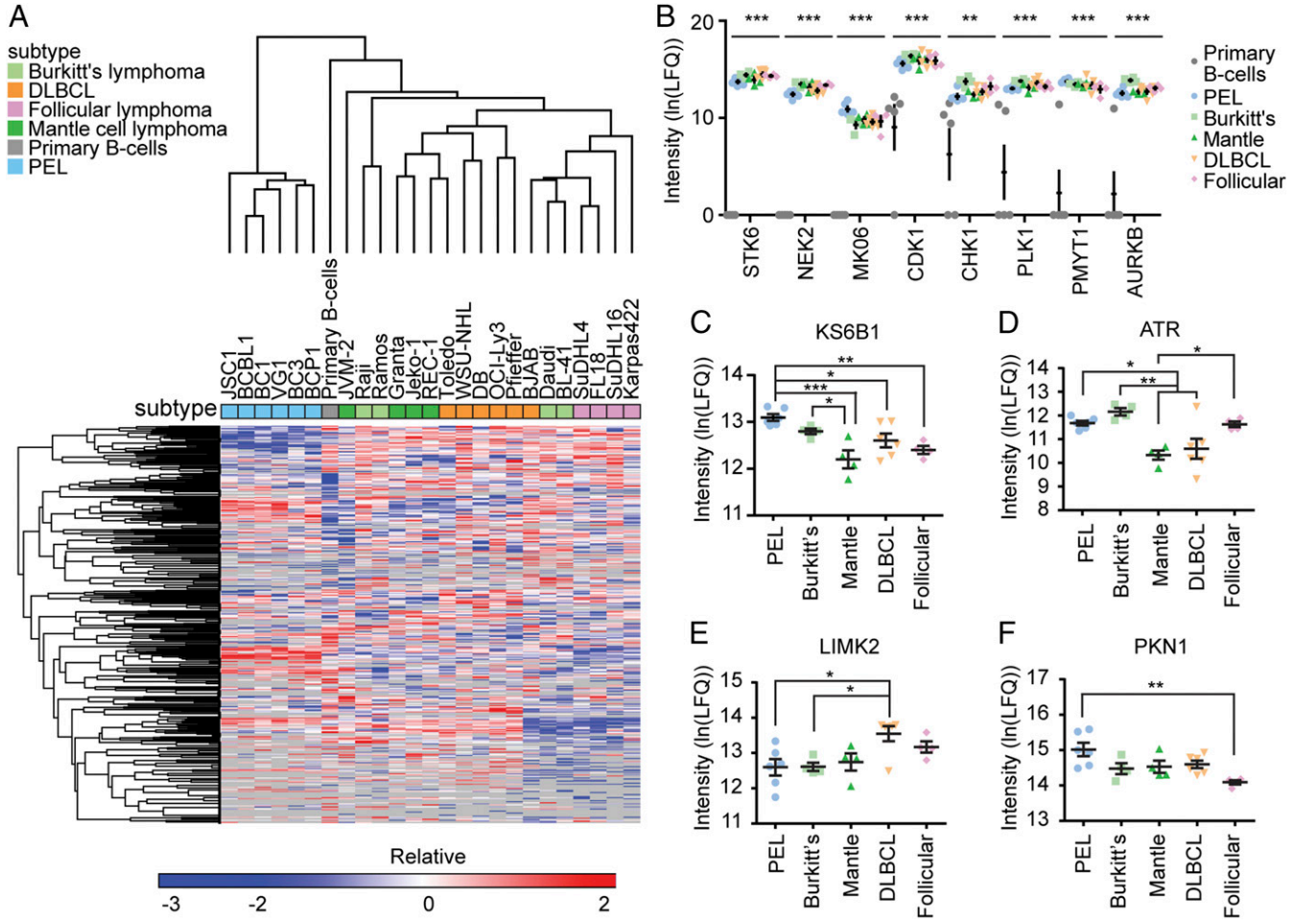

Fig. 1. The cellular kinome is more similar within subtypes than across subtypes. (*A*) Euclidian hierarchical clustering of 24 lymphoma cell lines from 5 subtypes and primary B cells that were subject to MIB/MS. Data presented are the average of 2 biological replicate MIB/MS runs for each cell line and the average of 5 replicate MIB/MS runs for primary B cells. Gray color indicates a kinase that was not captured in that cell line. (*B*) A select set of kinases having greater MIB binding in all cell lines relative to primary B cells is graphed. Points within each lymphoma subtype represent a single cell line. Points for primary B cells are from individual mass spectrometry runs. Data presented are the mean ± SEM with significance (ANOVA, $*P < 0.05$, $**P < 0.01$, $***P < 0.001$, degrees of freedom = 24) tested between primary B cells and each NHL subtype. Reported significance is the highest *P* value of all comparisons between each NHL subtype to the primary B cells. (*C*–*F*) A select set of kinases: (*C*) KS6B1, (*D*) ATR, (*E*) LIMK2, and (*F*) PKN1 displaying MIB-binding bias across subtypes. Each point represents a single cell line. Data presented are the mean ± SEM (ANOVA, $*P < 0.05$, $**P < 0.01$, $***P < 0.001$, degrees of freedom = 19). Refer to Dataset S2 for official gene names of the kinases. LFQ indicates label-free quantification.

in the follicular subtype (Fig. 1*F*). Euclidean hierarchical clustering analysis of kinases commonly activated in different NHL subtypes compared with primary B cells demonstrate PEL in general cluster together, while having lower functional MIB binding of RIOK2 and CHKA, but higher MIB binding of CDK16 compared with other NHL subtypes (Fig. 2).

Tyro3 Is Uniquely Up-Regulated in PEL. Large clusters of kinases in the PEL subtype displayed significantly greater or less MIB binding compared with all other NHL subtypes and primary B cells (Fig. 3*A*). Kinases significantly down-regulated in PEL include BTK, GSK3B, and TGFR1. This corresponds well to a previous report that PEL is insensitive to BTK inhibition, unlike DLBCL (31). Kinases up-regulated in PEL include KS6A1 (p90 S6K), KS6B1, and AKT2. KS6B1 and AKT2 are part of the phosphatidylinositol 3-kinase (PI3K)/protein kinase B (AKT)/mammalian target of rapamycin (mTOR) pathway, which has been shown to be important for PEL survival (32–34). Interestingly, Tyro3 was consistently captured by MIBs from all 6 PEL cell lines but absent from all other cell lines and primary B cells (Fig. 3*B*). Tyro3 is a member of the Tyro3/Axl/MerTK (TAM) receptor tyrosine kinase (RTK) family, whose overexpression promotes proliferation, survival, and chemoresistance

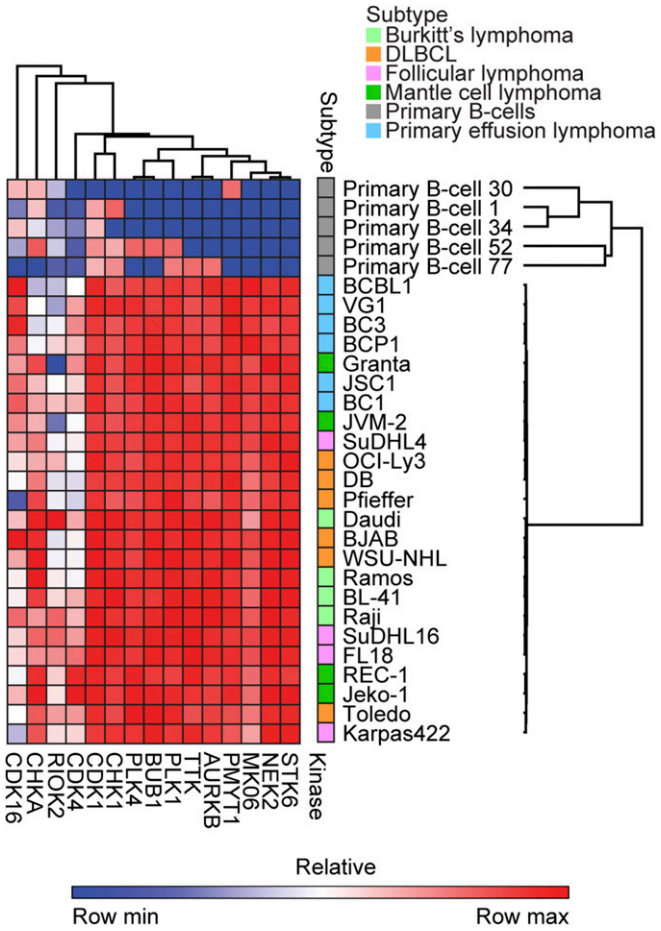

Fig. 2. A common set of kinases that are activated within NHL compared with primary B cells. Euclidian hierarchical clustering of kinases having statistically higher or lower MIB binding in NHL compared with primary B cells. Data presented are the average of 2 biological replicate MIB/MS runs for each cell line, while the data for primary B cells are MIB/MS runs pooled from different donors. Refer to Dataset S2 for official gene names of the kinases. Min indicates minimum; and max, maximum.

in solid cancers such as in melanoma, hepatocellular carcinoma, and colon cancer (35–38). MerTK, but not Axl or Tyro3, has also been shown to promote proliferation in multiple myeloma, which is a malignancy of plasmacytic origin (39). Transcriptional profiling by RNA-sequencing (seq) demonstrated *TYRO3* was uniquely transcriptionally up-regulated in PEL compared with all other subtypes (Fig. 3*C*) (40). In contrast, its related family members *AXL* and *MERTK* displayed a similar low level of expression across subtypes (Fig. 3 *D* and *E*). To confirm our expression data, we also examined expression levels of the TAM receptors and their ligands in a recent literature report by Journo et al. (41) that performed RNA-seq on BJAB, BCBL1, and BC3 cell lines. Trends in expression levels of these genes between cell lines were similar in both studies (*SI Appendix*, Fig. S2). PEL lines also exhibited high levels of Tyro3 protein expression in comparison with some other non-PEL NHL, which showed little to none (Fig. 3*F*). BC3, which had the lowest protein and mRNA levels of Tyro3 within the PEL subtype, nevertheless had greater MIB binding/activity in comparison with the cell lines from other subtypes. TAM receptors achieve maximal signaling when bound by the ligands Pros1 and/or Gas6 (42). Therefore, we examined if PEL also exhibit up-regulated expression of Pros1 or Gas6. PEL in general exhibited higher transcription levels of *PROS1*, but not *GAS6* compared with primary B cells (Fig. 3 *G* and *H*). To verify that the transcriptome obtained from PEL cell lines reflected the primary tumor, we harvested RNA from primary PEL patient samples to confirm if up-regulation of *TYRO3* transcripts held true in primary human samples. We observed significantly increased levels of *TYRO3*, *PROS1*, and *GAS6* mRNA transcripts in the PEL effusion ($n = 6$) in comparison with healthy primary B cells ($n = 7$) (Fig. 3*I*). Overall, our data demonstrate that Tyro3 and its activating ligand Pros1 are up-regulated in PEL cells.

Inhibition of Tyro3 Attenuates PI3K Signaling. During activation of an RTK, phosphorylation of tyrosine residues within the kinase domain results in propagation of a signaling cascade. We examined if Tyro3 was phosphorylated on its tyrosine residues, which would indicate the activation of Tyro3. Phospho-RTK arrays, which contain antibodies against a panel of RTKs including Tyro3, confirmed that Tyro3 was phosphorylated on tyrosine residues in PEL cells (BC1 and BCP1) in comparison with a DLBCL (BJAB), which exhibited none (Fig. 4*A*). In contrast, 1 kinase, ROR2, was commonly phosphorylated across all 3 cell lines. To confirm whether or not Tyro3 expression affects the activity of a downstream substrate in PEL cells, we examined if phosphorylation of the p85 regulatory subunit of PI3K, a known substrate of Tyro3, was affected upon knockdown of Tyro3 (43). We tested several short-hairpin (sh)RNA constructs against Tyro3 in PEL (BCBL1 and BC1) and DLBCL BJAB cells (*SI Appendix*, Fig. S3). Since shRNA clone 1527 negatively affected cell viability in PEL BCBL1 cells (*SI Appendix*, Fig. S3*B*), but had similar cell viability compared with the nontemplate control in DLBCL BJAB cells (*SI Appendix*, Fig. S3*D*), we proceeded with shRNA clone 1527 for further studies. Knockdown of Tyro3 in PEL, but not in BL, resulted in a decrease in tyrosine phosphorylation of p85 PI3K, consistent with a decrease in PI3K activity (Fig. 4*B*).

UNC3810A Is a Selective Kinase Inhibitor against Tyro3. The inclusion of TAM inhibitors to conventional therapies to allow chemotherapy to have a durable response may be helpful in treating cancers that often develop resistance to treatment. Currently there are several small molecule inhibitors that target the TAM receptors, but many of the compounds are pan-inhibitors of the Tyro3/Axl/MerTK family and frequently have a broad spectrum that includes MET and other RTKs (44, 45). We created a small molecule inhibitor with specificity toward Tyro3. Structure-activity studies of our MerTK inhibitors versus the TAM family led to UNC3810A

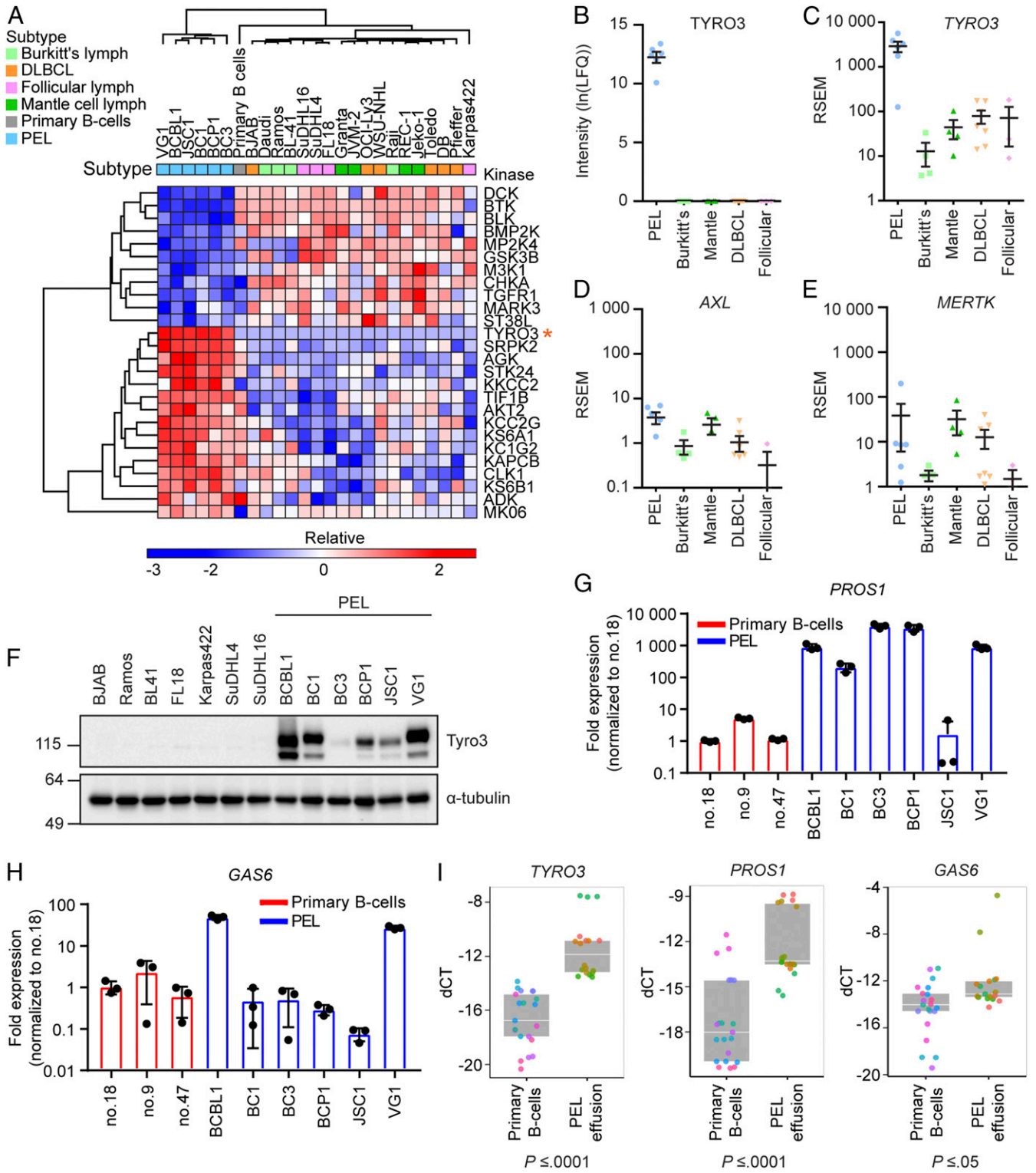

Fig. 3. Tyro3 is uniquely up-regulated in PEL. (*A*) Euclidian hierarchical clustering of kinases having statistically higher or lower MIB binding in PEL compared with all other samples combined. Data presented are the average of 2 biological replicate MIB/MS runs for each cell line and an average of 5 replicate MIB/MS runs for primary B cells. Orange asterisk (*) indicates the row containing Tyro3. Refer to Dataset S2 for official gene names of the kinases. (*B*) Tyro3 MIB-binding levels in each individual subtype. Each point represents 1 cell line. Data presented are the mean ± SEM. (*C*–*E*) mRNA expression of (*C*) *TYRO3*, (*D*) *AXL*, or (*E*) *MERTK* from RNA-seq in each individual subtype. Each point represents 1 cell line. Data presented are the mean ± SEM. (*F*) Western blot analysis of Tyro3 protein levels from different NHL subtypes. Representative of $n = 3$ independent experiments. (*G* and *H*) qRT-PCR analysis of (*G*) *PROS1* or (*H*) *GAS6* mRNA from PEL cell lines or primary B cells isolated from 3 different donors. Graph is representative of $n = 3$ independent experiments with different primary B cell donors used for each experiment. Bar graph represents the mean ± SD ($n = 3$). (*I*) qRT-PCR analysis of *TYRO3*, *PROS1*, or *GAS6* from primary B cells isolated from healthy donors ($n = 7$) or effusion from patients with PEL ($n = 6$). Replicates are shown as the same color for each primary B cell donor or PEL effusion sample. Data points are presented as the delta CT value between the gene of interest and actin for each individual replicate. Box plot represents the median with the 25th and 75th percentiles, respectively (ANOVA, *P* value listed below each graph). Lymph indicates lymphoma and LFQ indicates label-free quantification.

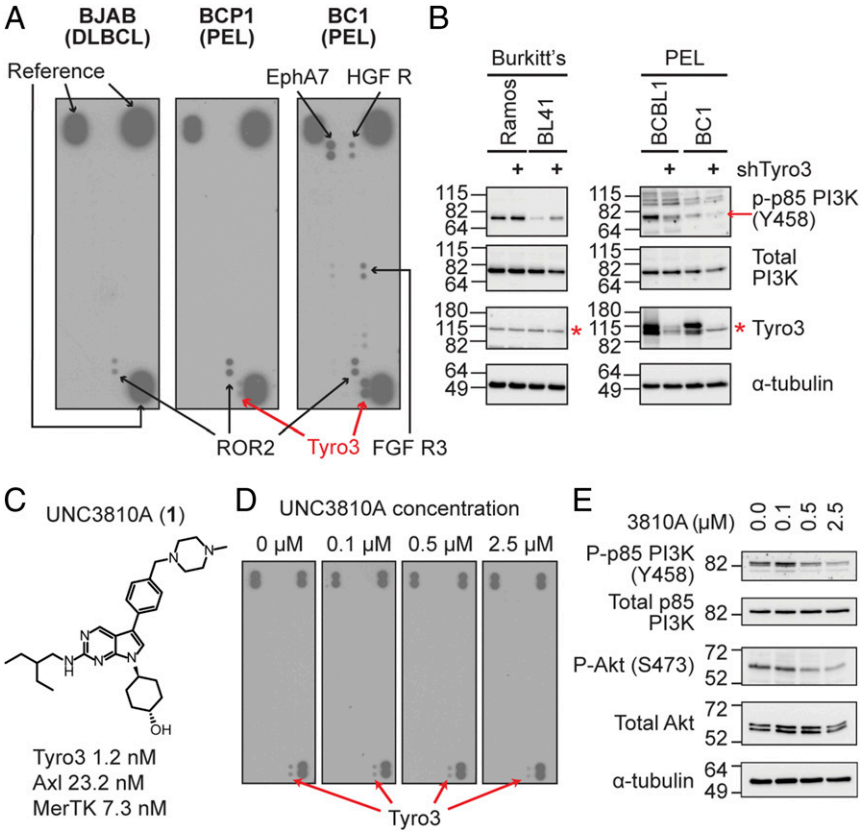

Fig. 4. Inhibition of Tyro3 results in attenuation of PI3K signaling. (*A*) Phospho-receptor tyrosine kinase (RTK) assay examining tyrosine phosphorylation of different RTKs. Reference spots are located at all corners except for the bottom left. (*B*) Western blot analysis of Burkitt's lymphoma or PEL cell lines stably knocked down with nontemplate control or Tyro3 shRNA. All cell lines were run on the same gel, but the blot was split in half for clarity due to different exposure times required to detect PI3K in Burkitt's compared with PEL cell lines. The red asterisk (*) indicates the location of a nonspecific band and the red arrow (→) indicates the p85 PI3K band. Representative of $n = 3$ independent experiments. (*C*) Structure of UNC3810A with IC_{50} values to the TAM family receptors. (*D*) Representative blot ($n = 2$ independent experiments) of a phospho-RTK assay with BCBL1 cells treated for 24 h with increasing concentrations of UNC3810A. Reference spots are located at all corners except for the bottom left. DMSO was used as the vehicle control. (*E*) Western blot analysis of the PI3K/Akt/mTOR signaling pathway in BCBL1 cells treated with increasing concentrations of UNC3810A for 24 h. DMSO was used as the vehicle control. Representative of $n = 3$ independent experiments.

(**1**), a pyrrolopyrimidine-based specific small molecule inhibitor against Tyro3 (Fig. 4*C* and *SI Appendix*, Fig. S4) (46). To determine the specificity of UNC3810A for Tyro3, we performed in vitro kinome selectivity profiling of UNC3810A against a wide array of kinases at 1 μM (*SI Appendix*, Fig. S5*A* and Dataset S3) and determined the IC_{50} of UNC3810A versus the TAM kinases, FLT3, and several additional targets that were inhibited by >80% at 1 μM (*SI Appendix*, Table S1). UNC3810A was most potent against Tyro3 (1.2 nM) and showed at least 10-fold selectivity versus all other kinases beyond MerTK, the most closely related TAM member, and TRKA. When examining the sensitivity of PEL cells to UNC3810A, most PEL lines exhibit an IC_{50} between 0.9 and 2.8 μM (*SI Appendix*, Fig. S5 *B* and *C*). Furthermore, PEL cell lines (BCBL1 and BC1) exhibited more sensitivity to UNC3810A in comparison with non-PEL cell lines (BJAB, Ramos, and BL41), which do not highly express Tyro3 (*SI Appendix*, Fig. S5*C*). Comparison of UNC3810A to a structurally related analog, which does not target Tyro3, UNC2369A, revealed that BCBL1 cells are more sensitive to UNC3810A compared with UNC2369A (*SI Appendix*, Fig. S5*D*) (46). UNC2369A is another pyrrolopyrimidine-based compound that is structurally similar to UNC3810A with an IC_{50} of 11 μM against Tyro3, 3.9 μM against Axl, and 400 nM against MerTK (see compound 20 from Zhang et al.) (46). To ensure these effects are not cell-type specific, we also examined the sensitivity of a colon cancer cell line, HT-29, and a melanoma cell line, B16-F10 to UNC3810A. Both colon cancer and melanoma have previously been shown to up-regulate Tyro3 to promote cell proliferation and chemoresistance (35, 37, 47, 48) and we confirmed HT-29 and B16-F10 express Tyro3 (*SI Appendix*, Fig. S5*E*). The sensitivity of both HT-29 and B16-F10 to UNC3810A was more similar to BCBL1 cells compared with BJAB cells (*SI Appendix*, Fig. S5*F*). To examine if UNC3810A also attenuated Tyro3-mediated PI3K signaling, we treated BCBL1 PEL cells with increasing amounts of UNC3810A. This resulted in a dose-dependent decrease of Tyro3 phosphorylation (Fig. 4*D*) and attenuated signaling through the PI3K/AKT/mTOR pathway as evidenced by decreased phosphorylation of p85 PI3K and AKT (Fig. 4*E*). Overall, these results suggest that UNC3810A is a selective inhibitor of Tyro3.

Inhibition of Tyro3 Results in Decreased Cell Survival. Tyro3 can activate the PI3K/AKT/mTOR pathway, whose inhibition in PEL cells results in cell death (32–34). If Tyro3 contributed to the activation of the PI3K/AKT/mTOR pathway, then reducing Tyro3 should affect PEL viability. We found that the PEL lines (BCBL1 and BC1) exhibited reduced cell viability in serum-starved conditions upon lentivirus-mediated shRNA knockdown of Tyro3 compared with cells transduced with a nontargeting control (NTC) shRNA (Fig. 5*A* and *SI Appendix*, Fig. S3*B*). These results suggest Tyro3 activates PI3K signaling to promote survival of PEL cells. Indicative of the lack of functionality of Tyro3 in non-PEL lines, knockdown of Tyro3 in 2 non-PEL cell lines, BJAB and BL41, had little to no effect on cell viability under the same conditions (Fig. 5*A* and *SI Appendix*, Fig. S3*D*). BCBL1 and BC1 PEL cells targeted with NTC shRNA or Tyro3 shRNA were also subjected to a colony formation assay, and the number of colonies formed by the Tyro3-depleted cells was significantly less than control cells (Fig. 5*B*). Similarly, treatment of PEL cell lines (BCBL1 and BC1) with UNC3810A also resulted in a significant attenuation in the formation of colonies for the PEL lines at 0.5 μM and 1 μM compared with the non-PEL NHL cell lines (BJAB, Ramos, and BL41), which exhibited none (Fig. 5 *C* and *D*).

Since PI3K and AKT phosphorylation levels decreased upon UNC3810A treatment, we examined if the PEL lines were more sensitive to UNC3810A compared with the other NHL subtypes. After treating cells for 72 h with 2 μM of UNC3810A or DMSO control, we measured cell growth using an MTS [3-(4,5-dimethylthiazol-2-yl)-5-(3-carboxymethoxyphenyl)-2-(4-sulfophenyl)-2*H*-tetrazolium] assay. PEL lines overall showed decreased cell

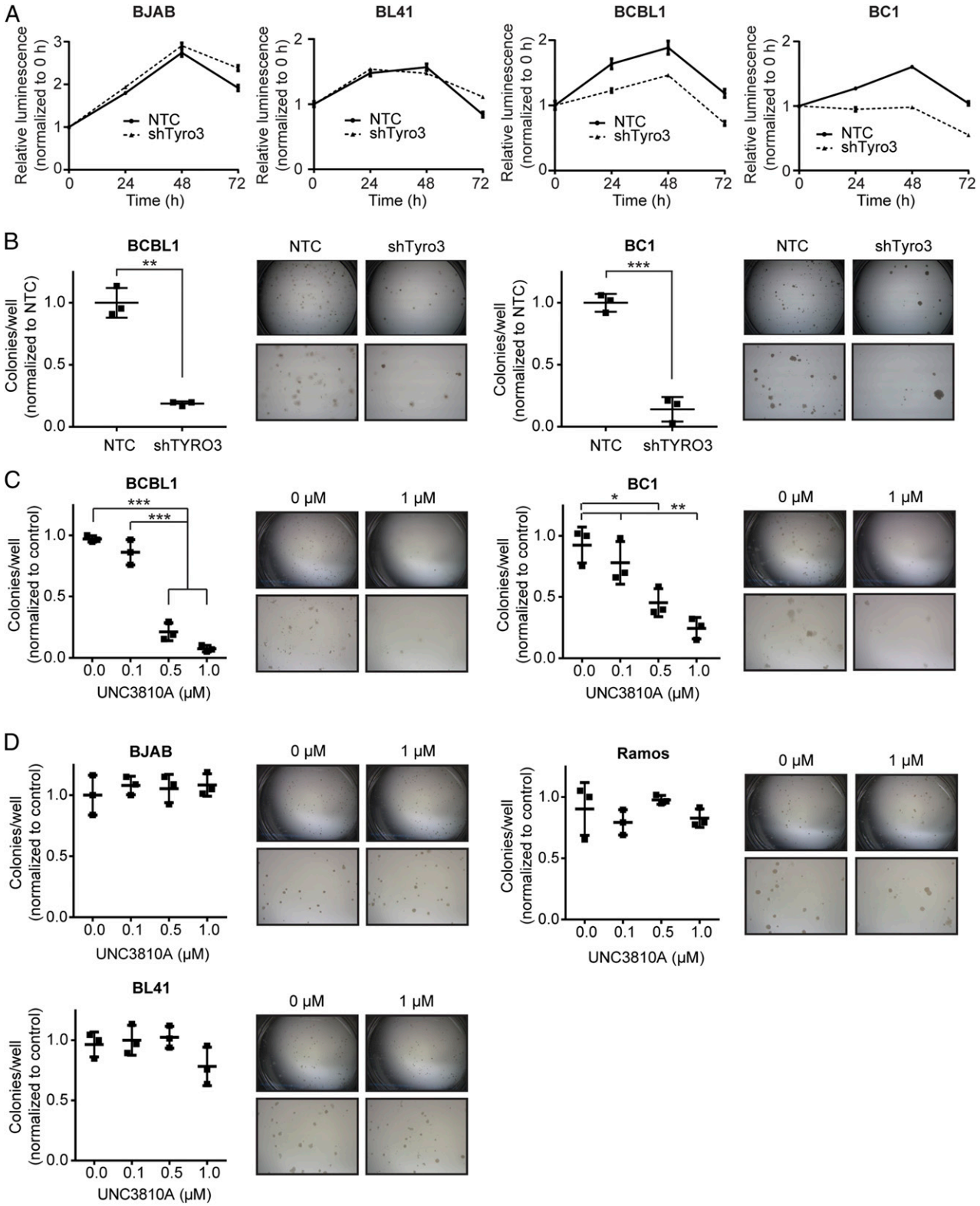

Fig. 5. Inhibition of Tyro3 results in a decrease of cell survival and colony formation in PEL. (*A*) Cell-Titer Glo analysis of non-PEL NHL or PEL cell lines stably knocked down with nontemplate control or Tyro3 shRNA over a time course of 72 h in serum-starved conditions. Luminescence was normalized to the reading at 0 h for each condition. (*B*) PEL cells were assessed for colony formation after being knocked down with nontemplate control or Tyro3 shRNA in a lentivirus-mediated manner. (*C* and *D*) Colony formation of (*C*) PEL (BCBL1 and BC1) or (*D*) non-PEL NHL (BJAB, Ramos, or BL41) cells was assessed over increasing concentrations of UNC3810A. Saline was used as the vehicle control. (*B–D*) Representative microscope pictures are shown capturing the full diameter of the tissue culture plate (lengthwise) and also an area enlarged at the middle. The diameter of each plate is 35 mm in length. Significance is calculated using a one-way ANOVA test (*$P < 0.05$, **$P < 0.01$, ***$P < 0.001$, degrees of freedom = 8). Pictures were taken with a Leica MZ6 light microscope attached with a Leica MC170 HD camera. (*A–D*) All quantitative data are presented as mean ± SD ($n = 3$ independent samples) and all experiments are representative of $n = 3$ independent experiments.

growth compared with all other NHL subtypes (Fig. 6*A*). We also examined if this inhibition of cellular proliferation in PEL cells is cytostatic or cytotoxic. After treatment of PEL cells with UNC3810A for 72 h, we found that cell viability decreased with increasing concentrations of UNC3810A (Fig. 6*B*). Apoptotic cell death can be mediated by active caspase-3, which cleaves many proteins upon activation, such as PARP. To determine if cell death occurred in a caspase-3 mediated manner, PEL cells were treated with UNC3810A for 72 h. A dose-dependent increase in caspase-3 activity was observed and corresponded with increased levels of cleaved caspase-3 (the active form of caspase-3) and PARP (Fig. 6 *C* and *D* and *SI Appendix*, Fig. S5*G*). We also examined if treating PEL cells with UNC3810A in combination with other inhibitors resulted in a further decrease in cell viability. Several studies have shown that the TAM receptors promote chemoresistance and that inhibition of the receptor(s) results in increased sensitivity to chemotherapy (35, 37, 49, 50). Hence, we investigated the efficacy of combined treatment of Tyro3 with 2 PI3K inhibitors, leniolisib and duvelisib, against PEL. We treated PEL lines with either UNC3810A, leniolisib, or together in combination for 72 h and measured cell viability. Treatment of PEL cells with both resulted in lower cell viability at multiple concentrations compared with treatment with either UNC3810A or leniolisib alone (*SI Appendix*, Fig. S6*A*). We also examined if treatment of PEL cells with another PI3K inhibitor, duvelisib, and UNC3810A in combination would have a similar effect. We saw there was a larger decrease in cell viability when treating with both inhibitors compared with either alone (*SI Appendix*, Fig. S6*B*). We also examined if either of these PI3K inhibitors were synergistic with UNC3810A. Using CompuSyn, we calculated the combination index (CI) at an effect level of 0.5 ($F_a = 0.5$) (51). In PEL cells, both drugs were synergistic (CI < 1) with UNC3810A though leniolisib was less synergistic with UNC3810A in comparison with duvelisib (*SI Appendix*, Fig. S6*C*).

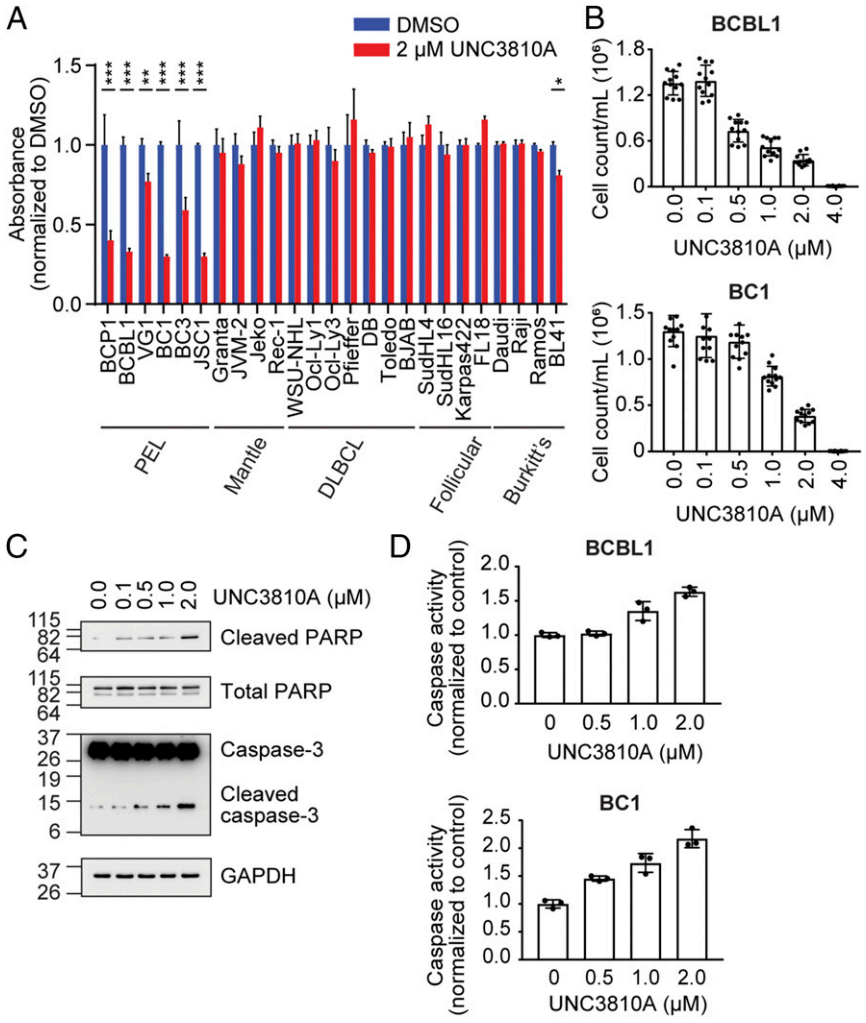

Fig. 6. UNC3810A treatment of PEL cells results in cell death. (*A*) Growth was measured using CellTiter 96 AQueous One solution from different NHL cell lines that were treated with 2 μM UNC3810A for 72 h. Absorbance readings in each cell line were normalized to the DMSO control from their respective cell line. Data are presented as mean ± SD ($n = 3$ independent wells) and are representative of $n = 3$ independent experiments (unpaired multiple *t* test by Holm–Sidak method, $^*P < 0.05$, $^{**}P < 0.01$, $^{***}P < 0.001$, degrees of freedom = 4). (*B*) PEL (BCBL1 and BC1) cells were treated with increasing concentrations of UNC3810A and harvested after 72 h of treatment. Cells were counted for viability using trypan blue. Saline was used as the vehicle control. Data are presented as mean ± SD ($n = 3$ independent samples, 4 counts from different 1-mm^2 areas on the hemocytometer per sample) and representative of $n = 3$ independent experiments. (*C*) Western blot analysis of caspase-3 activation in BC1 cells treated for 72 h with UNC3810A. Saline was used as the vehicle control. (*D*) Caspase-3 activity was measured in PEL (BCBL1 and BC1) cells treated with UNC3810A for 72 h using the ApoAlert fluorescent assay kit. Saline was used as the vehicle control. Data are presented as mean ± SD ($n = 3$ independent samples) and representative of $n = 3$ independent experiments.

These results suggest that addition of UNC3810A to this chemotherapeutic regimen may be beneficial.

UNC3810A Retards PEL Tumor Growth In Vivo. To determine if UNC3810A was efficacious in vivo, we examined if UNC3810A can attenuate tumor growth in a PEL xenograft mouse model. Using Trex-RTA BCBL1 cells, we introduced a constitutively active red-shifted luciferase (luc) gene thereby allowing us to monitor tumor growth upon addition of luciferin in the mice (52). To examine if UNC3810A would reach sufficient sustained plasma level concentrations, we performed a pharmacokinetic analysis of UNC3810A administered through an i.v., i.p., or oral route (*SI Appendix*, Fig. S7). Detectable plasma levels were sustained for 12 h when UNC3810A was administered through an i.p. route. At 25 mg/kg UNC3810A plasma concentration levels reached a maximum concentration of 5.72 μM (*SI Appendix*, Fig. S7*D*). After 4 wk of treatment at 25 mg/kg, tumor growth in mice treated with UNC3810A was significantly suppressed in comparison with the saline vehicle control group (Fig. 7 *A* and *B*). Control mice also had a significant amount of ascites (pleural effusion) collected from the peritoneal cavity compared with those treated with UNC3810A (Fig. 7*C*). Conversely in a BJAB xenograft mouse model on the same dosing regimen, there was no attenuation in tumor volume between mice treated with 25 mg/kg UNC3810A and the saline vehicle control (*SI Appendix*, Fig. S8). This correlated with the data from cell culture studies. Immunoblotting of the PEL tumors showed decreased levels of activating phosphorylation marks of S6 (Ser235/Ser236) in some of the mice treated with UNC3810A compared with those treated with the saline control (Fig. 7*D*). S6 is a ribosomal protein activated by the mTOR complex 1 (mTORC1) and phosphorylation of serine residues 235/236 are an indicator of active protein translation. Confirming these results, immunohistochemistry analysis of these solid tumors showed decreased levels of activated AKT (Thr308) and ribosomal S6 (Ser236/236) in mice treated with UNC3810A compared with mice treated with the saline control (Fig. 7*E* and *SI Appendix*, Fig. S9). The activation of AKT can promote cell survival and the activation of S6 can promote protein synthesis. Therefore, tumors in mice treated with UNC3810A may exhibit delayed tumor progression due to inhibition of Tyro3 and several survival pathways influenced by AKT.

Discussion

Kinases control the activity of many cellular pathways and are the target of the fastest growing class of FDA-approved oncology drugs (53). Performing MIB-based kinome profiling allows us to interrogate the kinome using a proteomic-based approach to identify expressed and activated kinases in the cell (21). Overexpression of a kinase does not necessarily correlate to its activity (54, 55), therefore characterizing the activity of kinases can identify candidate kinases, which may not be considered a hit from more traditional genomic and transcriptomic approaches. In the case of PEL (and other virally associated cancers), expression of viral proteins or microRNAs can mediate the activation or repression of host kinases in signaling pathways (56, 57).

To identify possible targets of interest, we kinome profiled key NHL subtypes and identified kinases whose activity was specifically up-regulated in one or a few subtypes. The most significant hit in the kinome profiling screen for PEL was Tyro3, whose

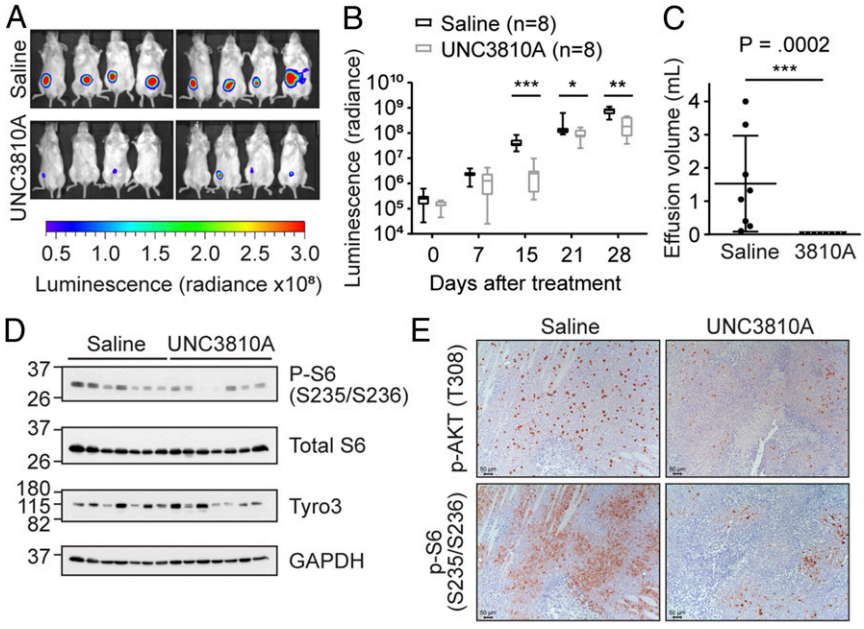

Fig. 7. UNC3810A retards PEL tumor growth in vivo. NOD-SCID mice in a BCBL1-PEL xenograft model were i.p. injected with 0.9% saline (control) or 25 mg/kg UNC3810A 3 times a week—Monday, Wednesday, and Friday (MWF) over a course of 4 wk (n = 8 mice per group). Luciferase expression in saline or UNC3810A-treated mice was measured weekly by i.p. injecting mice with luciferin. (*A*) Luminescence images representing tumor burden taken at a 1-min exposure at 15 d after start of treatment. Luminescence images depict photon emission from tissue and are expressed as radiance (photons/second/centimeter squared/steradian). (*B*) Luminescence images were quantified using Living Image v4.4 to measure photon emission from tissue and are expressed as radiance (photons/second/centimeter squared/steradian). Data are presented as a box and whiskers plot with the whiskers marking the minimum and maximum values. The lowest, middle, and top lines of the box, respectively, represent the 25th percentile, median, and 75th percentile. (*C*) Effusions collected from mice treated with saline or UNC3810A were measured at the end of the study. Data represent mean ± SD (n = 8 mice per group). (*D*) Western blot analysis of solid tumors from mice treated with saline or UNC3810A (n = 7 per group). (*E*) Representative pictures of immunohistochemistry (IHC) stains against p-AKT (Thr308) and p-S6 (Ser235/Ser236) of mice treated with saline or UNC3810A. Sections were developed with DAB (3,3′-diaminobenzidine) and counterstained with hematoxylin. (Scale bars, 50 μm.) Slides were imaged using a Leica microscope (DMLS) and camera (DMC2900), and acquired using the Leica Application Suite v4.8 software. For *B* and *C* a 2-tailed unpaired Mann–Whitney *U* test was used to determine significance (*P < 0.05, **P < 0.01, ***P < 0.001).

up-regulation in other cancers promotes survival and resistance to chemotherapy (35–38). Tyro3 can activate several pathways, including the PI3K/AKT/mTOR pathway, whose activity is important for PEL survival (32–34, 58). Interestingly in Kaposi's sarcoma (KS), another KSHV-mediated malignancy, Axl was up-regulated and shown to drive PI3K signaling (59). Knockdown of Axl resulted in an attenuation of cell growth and invasion in KS cell lines. In normal B cells, expression of TAM receptors is very low or absent (49, 50, 60). Of the subtypes screened, only PEL showed high expression and activity of Tyro3. We then developed a Tyro3-specific inhibitor, UNC3810A. In multiple cell culture assays, signaling and viability was inhibited by UNC3810A in PEL cell lines expressing Tyro3 while NHL cell lines with low or absent levels of Tyro3 were not significantly altered. Further testing in xenograft models demonstrated that treatment of PEL bearing mice with UNC3810A resulted in a lower tumor burden compared with the saline control that was not seen in a non-PEL NHL model. These data provide proof of principle that targeting Tyro3 may be effective in treating PEL.

Several studies have looked at the efficacy of using inhibitors to the PI3K/AKT/mTOR pathway in the treatment of PEL (32–34, 61–63). Since several other NHL subtypes have been shown to develop resistance to PI3K inhibition (64–66), inhibition of Tyro3 may be more beneficial than just targeting PI3K as Tyro3 can signal into multiple pathways, including the MAPK/extracellular-signal-regulated kinase (ERK) (67–70), p38 MAPK (71), Janus kinase (JAK)/signal transducer of activation (STAT) (42), and phospholipase C (PLC) pathways (42, 70). Both the MAPK/ERK and p38 MAPK pathways are activated in KSHV-infected PEL (72–74). Furthermore, KSHV also encodes a viral homolog of interleukin-6 (vIL-6), which can activate the JAK/STAT pathway similar to cellular IL-6 (56). Since Tyro3 signals through several pathways activated in KSHV-associated malignancies, inhibiting Tyro3 may be more efficacious than inhibiting PI3K alone. Furthermore, as expression of Tyro3 in other cancers has been shown to promote resistance to chemotherapy, which is a major obstacle in treating PEL, addition of a Tyro3 inhibitor may help sensitize cells to chemotherapy (35, 36). We observed that treatment of PEL cells with UNC3810A in conjunction with the PI3K inhibitors, leniolisib and duvelisib, inhibited cell viability to a higher degree compared with either treatment alone. Further studies with Tyro3 inhibitors in PEL either as single agent or in the adjuvant setting are warranted.

In this study, we only focused on the role of Tyro3 in PEL, but our screen uncovered additional differentially activated kinases. For example, DLBCL exhibited higher activity of LIMK2 compared with other subtypes. LIMK2 has been shown to play a role in pancreatic cancer metastasis (75). Whether LIMK2 activity is an indicator or predictor of aggressiveness in DLBCL is of interest. Our combined study of kinome profiling coupled with Tyro3 inhibitor development revealed that the kinome profiles between NHL subtypes contain significant differences, and that the interrogation of the kinome may help identify specific pathways that are important for survival or pathogenesis in tumors. This approach is useful in devising personalized therapies for different subsets of NHL, as well as many other solid and hematological cancers.

Materials and Methods

Mice. NOD-SCID gamma (NSG) mice used in the BCBL1 and BJAB xenograft studies were maintained in pathogen-free conditions and the studies were approved by the Institutional Animal Care and Use Committee (IACUC) at the University of North Carolina at Chapel Hill. The 4- to 5-wk-old NSG female mice weighing ∼20 g used in the xenograft studies were purchased from The Jackson Laboratory (005557). The pharmacokinetic (PK) analysis was completed by Sai Life Sciences Limited. The study was conducted in accordance with guidelines provided by the Committee for the Purpose of Control and Supervision of Experiments on Animals (CPCSEA) as published in The Gazette of India (1998) and approved by the Institutional Animal Ethics Committee (IAEC). The 8- to 12-wk-old Swiss Albino male mice weighing ∼25 to 35 g used in the PK study were purchased from Global, India.

Cell Culture. Except for OCI-Ly1 and OCI-Ly3, NHL cell lines were grown in a similar manner as described previously (33, 76, 77). OCI-Ly1 and OCI-Ly3 were grown in Iscove's modified Dulbecco's medium (IMDM), 20% human AB serum (Sigma-Aldrich, H4522), 1% penicillin–streptomycin, and 75 μM β-mercaptoethanol (Gibco, 21985-023). Please see *SI Appendix* for more details for other cell lines.

MIB/MS Affinity Chromatography. MIB/MS profiling was performed in a similar manner as previously described (78). Please see *SI Appendix* for more details.

Synthesis of UNC3810A (1). Please see *SI Appendix* for a detailed synthesis of UNC3810A. For NMR and mass spectrometry (ESI) data of the intermediates and UNC3810A please refer to *SI Appendix*, Fig. S4.

Statistical Analysis. Statistical tests applied in this study used either GraphPad Prism 7.02 or R with P values <0.05 considered significant.

Data Availability. The RNA-seq data reported in this study are deposited in the GEO database under the accession no. GSE114791. The mass spectrometry proteomics data from the MIB/MS profiling are deposited in the ProteomeXchange Consortium by the PRIDE (79) partner repository with the dataset identifier PXD012087.

ACKNOWLEDGMENTS. We thank the members of the B.D. and D.P.D. labs for helpful discussions, the UNC Lineberger Animal Studies Core for performing animal studies, and the UNC Animal Histopathology & Lab Medicine Core. We thank Ricardo Rivera-Soto for his help with the synergy experiments. This work was supported in part by the National Cancer Institute Center Core Support Grant CA16086 and 5P30CA016086 to the UNC Lineberger Comprehensive Cancer Center for the UNC Lineberger Animal Studies Core and the UNC Animal Histopathology & Lab Medicine Core, respectively. We also thank the AIDS and Cancer Specimen Resource (ACSR) for providing effusions from patients with PEL. We thank Jae Jung for providing the Trex-RTA BCBL1 cells. This work was supported by public health service grants CA096500 and CA163217 and a Leukemia and Lymphoma Quest for Cures grant. B.D. is a Leukemia and Lymphoma Society Scholar, and a Burroughs Wellcome Fund Investigator in Infectious Disease. This work was also supported in part by the National Institutes of Health Virology Training Grant T32 AI007419 (to J.P.W.), the University Cancer Research Fund and Federal Funds from the National Cancer Institute, National Institute of Health, under Contract HHSN261200800001E for medicinal chemistry efforts (to X.W., J.Z., W.Z., and S.V.F.), NIH Grant U24DK116204 (to G.L.J.), and NIH Grant CA019014 (to D.P.D.).

1. E. Boulanger *et al.*, Prognostic factors and outcome of human herpesvirus 8-associated primary effusion lymphoma in patients with AIDS. *J. Clin. Oncol.* **23**, 4372–4380 (2005).
2. S. Guillet *et al.*, Classic and extracavitary primary effusion lymphoma in 51 HIV-infected patients from a single institution. *Am. J. Hematol.* **91**, 233–237 (2016).
3. P. H. Goncalves, J. Ziegelbauer, T. S. Uldrick, R. Yarchoan, Kaposi sarcoma herpesvirus-associated cancers and related diseases. *Curr. Opin. HIV AIDS* **12**, 47–56 (2016).
4. E. Boulanger, V. Meignin, E. Oksenhendler, Bortezomib (PS-341) in patients with human herpesvirus 8-associated primary effusion lymphoma. *Br. J. Haematol.* **141**, 559–561 (2008).
5. T. Siddiqi, R. M. Joyce, A case of HIV-negative primary effusion lymphoma treated with bortezomib, pegylated liposomal doxorubicin, and rituximab. *Clin. Lymphoma Myeloma* **8**, 300–304 (2008).
6. A. Gupta, S. Sen, E. Marley, W. Chen, H. V. Naina, Management and outcomes of HIV-associated primary effusion lymphoma: A single center experience. *Clin. Lymphoma Myeloma Leuk.* **16** (suppl.), S175–S180 (2016).
7. S. G. O'Brien *et al.*; IRIS Investigators, Imatinib compared with interferon and low-dose cytarabine for newly diagnosed chronic-phase chronic myeloid leukemia. *N. Engl. J. Med.* **348**, 994–1004 (2003).
8. A. A. Alizadeh *et al.*, Distinct types of diffuse large B-cell lymphoma identified by gene expression profiling. *Nature* **403**, 503–511 (2000).
9. J. J. Yunis *et al.*, Distinctive chromosomal abnormalities in histologic subtypes of non-Hodgkin's lymphoma. *N. Engl. J. Med.* **307**, 1231–1236 (1982).
10. L. M. Weiss, R. A. Warnke, J. Sklar, M. L. Cleary, Molecular analysis of the t(14;18) chromosomal translocation in malignant lymphomas. *N. Engl. J. Med.* **317**, 1185–1189 (1987).
11. R. Rimokh *et al.*, Detection of the chromosomal translocation t(11;14) by polymerase chain reaction in mantle cell lymphomas. *Blood* **83**, 1871–1875 (1994).
12. J. Y. Li *et al.*, Detection of translocation t(11;14)(q13;q32) in mantle cell lymphoma by fluorescence in situ hybridization. *Am. J. Pathol.* **154**, 1449–1452 (1999).

13. M. Arguello *et al*., Disruption of the B-cell specific transcriptional program in HHV-8 associated primary effusion lymphoma cell lines. *Oncogene* **22**, 964–973 (2003).
14. R. C. Rickert, New insights into pre-BCR and BCR signalling with relevance to B cell malignancies. *Nat. Rev. Immunol.* **13**, 578–591 (2013).
15. L. Zech, U. Haglund, K. Nilsson, G. Klein, Characteristic chromosomal abnormalities in biopsies and lymphoid-cell lines from patients with Burkitt and non-Burkitt lymphomas. *Int. J. Cancer* **17**, 47–56 (1976).
16. R. Taub *et al*., Translocation of the c-myc gene into the immunoglobulin heavy chain locus in human Burkitt lymphoma and murine plasmacytoma cells. *Proc. Natl. Acad. Sci. U.S.A.* **79**, 7837–7841 (1982).
17. A. B. Eason *et al*., Differential IgM expression distinguishes two types of pediatric Burkitt lymphoma in mouse and human. *Oncotarget* **7**, 63504–63513 (2016).
18. R. G. Jenner *et al*., Kaposi's sarcoma-associated herpesvirus-infected primary effusion lymphoma has a plasma cell gene expression profile. *Proc. Natl. Acad. Sci. U.S.A.* **100**, 10399–10404 (2003).
19. U. Klein *et al*., Gene expression profile analysis of AIDS-related primary effusion lymphoma (PEL) suggests a plasmablastic derivation and identifies PEL-specific transcripts. *Blood* **101**, 4115–4121 (2003).
20. E. Cesarman, Y. Chang, P. S. Moore, J. W. Said, D. M. Knowles, Kaposi's sarcoma-associated herpesvirus-like DNA sequences in AIDS-related body-cavity-based lymphomas. *N. Engl. J. Med.* **332**, 1186–1191 (1995).
21. J. S. Duncan *et al*., Dynamic reprogramming of the kinome in response to targeted MEK inhibition in triple-negative breast cancer. *Cell* **149**, 307–321 (2012).
22. J. P. Wong *et al*., Kinome profiling of non-Hodgkin lymphoma identifies Tyro3 as a therapeutic target in PEL. PRIDE Archive. https://www.ebi.ac.uk/pride/archive/projects/PXD012087. Deposited 17 December 2018.
23. K. S. Elenitoba-Johnson *et al*., Involvement of multiple signaling pathways in follicular lymphoma transformation: p38-mitogen-activated protein kinase as a target for therapy. *Proc. Natl. Acad. Sci. U.S.A.* **100**, 7259–7264 (2003).
24. I. S. Lossos, R. D. Gascoyne, Transformation of follicular lymphoma. *Best Pract. Res. Clin. Haematol.* **24**, 147–163 (2011).
25. J. N. Winter, D. Variakojis, A. L. Epstein, Phenotypic analysis of established diffuse histiocytic lymphoma cell lines utilizing monoclonal antibodies and cytochemical techniques. *Blood* **63**, 140–146 (1984).
26. H. Taji *et al*., Growth inhibition of CD20-positive B lymphoma cell lines by IDEC-C2B8 anti-CD20 monoclonal antibody. *Jpn. J. Cancer Res.* **89**, 748–756 (1998).
27. S. Morelli *et al*., Oligonucleotides induce apoptosis restricted to the t(14;18) DHL-4 cell line. *Anticancer Drug Des.* **11**, 1–14 (1996).
28. M. J. Dyer, P. Fischer, E. Nacheva, W. Labastide, A. Karpas, A new human B-cell non-Hodgkin's lymphoma cell line (Karpas 422) exhibiting both t (14;18) and t(4;11) chromosomal translocations. *Blood* **75**, 709–714 (1990).
29. N. Di Gaetano *et al*., Synergism between fludarabine and rituximab revealed in a follicular lymphoma cell line resistant to the cytotoxic activity of either drug alone. *Br. J. Haematol.* **114**, 800–809 (2001).
30. P. J. Brown *et al*., Potentially oncogenic B-cell activation-induced smaller isoforms of FOXP1 are highly expressed in the activated B cell-like subtype of DLBCL. *Blood* **111**, 2816–2824 (2008).
31. L. Bonsignore *et al*., A role for MALT1 activity in Kaposi's sarcoma-associated herpes virus latency and growth of primary effusion lymphoma. *Leukemia* **31**, 614–624 (2017).
32. S. H. Sin *et al*., Rapamycin is efficacious against primary effusion lymphoma (PEL) cell lines in vivo by inhibiting autocrine signaling. *Blood* **109**, 2165–2173 (2007).
33. A. P. Bhatt *et al*., Dual inhibition of PI3K and mTOR inhibits autocrine and paracrine proliferative loops in PI3K/Akt/mTOR-addicted lymphomas. *Blood* **115**, 4455–4463 (2010).
34. S. Uddin *et al*., Inhibition of phosphatidylinositol 3′-kinase/AKT signaling promotes apoptosis of primary effusion lymphoma cells. *Clin. Cancer Res.* **11**, 3102–3108 (2005).
35. C. W. Chien *et al*., Targeting TYRO3 inhibits epithelial-mesenchymal transition and increases drug sensitivity in colon cancer. *Oncogene* **35**, 5872–5881 (2016).
36. T. D. Kabir *et al*., A microRNA-7/growth arrest specific 6/TYRO3 axis regulates the growth and invasiveness of sorafenib-resistant cells in human hepatocellular carcinoma. *Hepatology* **67**, 216–231 (2018).
37. S. Zhu *et al*., A genomic screen identifies TYRO3 as a MITF regulator in melanoma. *Proc. Natl. Acad. Sci. U.S.A.* **106**, 17025–17030 (2009).
38. Y. Duan *et al*., Overexpression of Tyro3 and its implications on hepatocellular carcinoma progression. *Int. J. Oncol.* **48**, 358–366 (2016).
39. J. S. Waizenegger *et al*., Role of growth arrest-specific gene 6-Mer axis in multiple myeloma. *Leukemia* **29**, 696–704 (2015).
40. J. P. Wong *et al*., Kinome profiling of non-Hodgkin's lymphoma reveals Tyro3 is important in primary effusion lymphoma survival. Gene Expression Omnibus. https://www.ncbi.nlm.nih.gov/geo/query/acc.cgi?acc=GSE114791. Deposited 22 May 2018.
41. G. Journo *et al*., Modulation of cellular CpG DNA methylation by Kaposi's sarcoma-associated herpesvirus. *J. Virol.* **92**, e00008-18 (2018).
42. W. I. Tsou *et al*., Receptor tyrosine kinases, TYRO3, AXL, and MER, demonstrate distinct patterns and complex regulation of ligand-induced activation. *J. Biol. Chem.* **289**, 25750–25763 (2014).
43. Z. Lan *et al*., Transforming activity of receptor tyrosine kinase tyro3 is mediated, at least in part, by the PI3 kinase-signaling pathway. *Blood* **95**, 633–638 (2000).
44. D. K. Graham, D. DeRyckere, K. D. Davies, H. S. Earp, The TAM family: Phosphatidylserine sensing receptor tyrosine kinases gone awry in cancer. *Nat. Rev. Cancer* **14**, 769–785 (2014).
45. T. Baladi, V. Abet, S. Piguel, State-of-the-art of small molecule inhibitors of the TAM family: The point of view of the chemist. *Eur. J. Med. Chem.* **105**, 220–237 (2015).
46. W. Zhang *et al*., UNC2025, a potent and orally bioavailable MER/FLT3 dual inhibitor. *J. Med. Chem.* **57**, 7031–7041 (2014).
47. R. Schmitz *et al*., TAM receptors Tyro3 and Mer as novel targets in colorectal cancer. *Oncotarget* **7**, 56355–56370 (2016).
48. S. J. Demarest *et al*., Evaluation of Tyro3 expression, Gas6-mediated Akt phosphorylation, and the impact of anti-Tyro3 antibodies in melanoma cell lines. *Biochemistry* **52**, 3102–3118 (2013).
49. S. Sinha *et al*., Targeted Axl inhibition primes chronic lymphocytic leukemia B Cells to apoptosis and shows synergistic/additive effects in combination with BTK inhibitors. *Clin. Cancer Res.* **21**, 2115–2126 (2015).
50. R. M. Linger *et al*., Mer receptor tyrosine kinase is a therapeutic target in pre-B-cell acute lymphoblastic leukemia. *Blood* **122**, 1599–1609 (2013).
51. T. C. Chou, N. Martin, *CompuSyn for Drug Combinations: PC Software and User's Guide: A Computer Program for Quantitation of Synergism and Antagonism in Drug Combinations, and the Determination of IC50 and ED50 and LD50 Values* (ComboSyn Inc, Paramus, NJ, 2005).
52. H. Nakamura *et al*., Global changes in Kaposi's sarcoma-associated virus gene expression patterns following expression of a tetracycline-inducible Rta transactivator. *J. Virol.* **77**, 4205–4220 (2003).
53. P. Wu, T. E. Nielsen, M. H. Clausen, Small-molecule kinase inhibitors: An analysis of FDA-approved drugs. *Drug Discov. Today* **21**, 5–10 (2016).
54. M. P. Lutz *et al*., Overexpression and activation of the tyrosine kinase Src in human pancreatic carcinoma. *Biochem. Biophys. Res. Commun.* **243**, 503–508 (1998).
55. H. Mueller *et al*., Potential prognostic value of mitogen-activated protein kinase activity for disease-free survival of primary breast cancer patients. *Int. J. Cancer* **89**, 384–388 (2000).
56. L. Giffin, B. Damania, KSHV: Pathways to tumorigenesis and persistent infection. *Adv. Virus Res.* **88**, 111–159 (2014).
57. D. P. Dittmer, B. Damania, Kaposi sarcoma-associated herpesvirus: Immunobiology, oncogenesis, and therapy. *J. Clin. Invest.* **126**, 3165–3175 (2016).
58. R. M. Linger, A. K. Keating, H. S. Earp, D. K. Graham, TAM receptor tyrosine kinases: Biologic functions, signaling, and potential therapeutic targeting in human cancer. *Adv. Cancer Res.* **100**, 35–83 (2008).
59. R. Liu *et al*., Induction, regulation, and biologic function of Axl receptor tyrosine kinase in Kaposi sarcoma. *Blood* **116**, 297–305 (2010).
60. A. Neubauer *et al*., Expression of axl, a transforming receptor tyrosine kinase, in normal and malignant hematopoiesis. *Blood* **84**, 1931–1941 (1994).
61. M. Granato *et al*., Quercetin induces apoptosis and autophagy in primary effusion lymphoma cells by inhibiting PI3K/AKT/mTOR and STAT3 signaling pathways. *J. Nutr. Biochem.* **41**, 124–136 (2017).
62. L. Mediani *et al*., Reversal of the glycolytic phenotype of primary effusion lymphoma cells by combined targeting of cellular metabolism and PI3K/Akt/mTOR signaling. *Oncotarget* **7**, 5521–5537 (2016).
63. P. Gasperini, G. Tosato, Targeting the mammalian target of Rapamycin to inhibit VEGF and cytokines for the treatment of primary effusion lymphoma. *Leukemia* **23**, 1867–1874 (2009).
64. S. Iyengar *et al*., P110α-mediated constitutive PI3K signaling limits the efficacy of p110δ-selective inhibition in mantle cell lymphoma, particularly with multiple relapse. *Blood* **121**, 2274–2284 (2013).
65. J. H. Kim, W. S. Kim, K. J. Ryu, S. J. Kim, C. Park, CXCR4 can induce PI3Kδ inhibitor resistance in ABC DLBCL. *Blood Cancer J.* **8**, 23 (2018).
66. K. Walsh *et al*., PAK1 mediates resistance to PI3K inhibition in lymphomas. *Clin. Cancer Res.* **19**, 1106–1115 (2013).
67. M. Katagiri *et al*., Mechanism of stimulation of osteoclastic bone resorption through Gas6/Tyro 3, a receptor tyrosine kinase signaling, in mouse osteoclasts. *J. Biol. Chem.* **276**, 7376–7382 (2001).
68. J. E. Brown, M. Krodel, M. Pazos, C. Lai, A. L. Prieto, Cross-phosphorylation, signaling and proliferative functions of the Tyro3 and Axl receptors in Rat2 cells. *PLoS One* **7**, e36800 (2012).
69. A. L. Prieto, S. O'Dell, B. Varnum, C. Lai, Localization and signaling of the receptor protein tyrosine kinase Tyro3 in cortical and hippocampal neurons. *Neuroscience* **150**, 319–334 (2007).
70. K. Fujita *et al*., Targeting Tyro3 ameliorates a model of PGRN-mutant FTLD-TDP via tau-mediated synaptic pathology. *Nat. Commun.* **9**, 433 (2018).
71. H. J. Park, J. Y. Baen, Y. J. Lee, Y. H. Choi, J. L. Kang, The TAM-family receptor Mer mediates production of HGF through the RhoA-dependent pathway in response to apoptotic cells. *Mol. Biol. Cell* **23**, 3254–3265 (2012).
72. N. Sharma-Walia *et al*., ERK1/2 and MEK1/2 induced by Kaposi's sarcoma-associated herpesvirus (human herpesvirus 8) early during infection of target cells are essential for expression of viral genes and for establishment of infection. *J. Virol.* **79**, 10308–10329 (2005).
73. H. Pan, J. Xie, F. Ye, S. J. Gao, Modulation of Kaposi's sarcoma-associated herpesvirus infection and replication by MEK/ERK, JNK, and p38 multiple mitogen-activated protein kinase pathways during primary infection. *J. Virol.* **80**, 5371–5382 (2006).
74. J. Xie, A. O. Ajibade, F. Ye, K. Kuhne, S. J. Gao, Reactivation of Kaposi's sarcoma-associated herpesvirus from latency requires MEK/ERK, JNK and p38 multiple mitogen-activated protein kinase pathways. *Virology* **371**, 139–154 (2008).
75. D. H. Vlecken, C. P. Bagowski, LIMK1 and LIMK2 are important for metastatic behavior and tumor cell-induced angiogenesis of pancreatic cancer cells. *Zebrafish* **6**, 433–439 (2009).
76. L. Giffin, J. A. West, B. Damania, Kaposi's sarcoma-associated herpesvirus interleukin-6 modulates endothelial cell movement by upregulating cellular genes involved in migration. *MBio* **6**, e01499-15 (2015).
77. A. P. Bhatt *et al*., Dysregulation of fatty acid synthesis and glycolysis in non-Hodgkin lymphoma. *Proc. Natl. Acad. Sci. U.S.A.* **109**, 11818–11823 (2012).
78. T. J. Stuhlmiller *et al*., Kinome and transcriptome profiling reveal broad and distinct activities of erlotinib, sunitinib, and sorafenib in the mouse heart and suggest cardiotoxicity from combined signal transducer and activator of transcription and epidermal growth factor receptor inhibition. *J. Am. Heart Assoc.* **6**, e006635 (2017).
79. J. A. Vizcaíno *et al*., 2016 update of the PRIDE database and its related tools. *Nucleic Acids Res.* **44**, D447–D456 (2016).